

Synthesis of Ultradispersed Nickel Particles by Reduction of High-Loaded NiO–SiO₂ Systems Prepared by Heterophase Sol–Gel Method

Marina A. Ermakova,* D. Yu. Ermakov, S. V. Cherepanova, and L. M. Plyasova

*Boriskov Institute of Catalysis, Siberian Branch of the Russian Academy of Sciences,
Prospekt Ak. Lavrentieva 5, Novosibirsk 630090, Russia*

Received: May 16, 2002; In Final Form: July 30, 2002

TPR, XRD, TEM, and IR techniques were used for studying reduction of nickel–silica systems over the whole concentration range (nickel content was varied within the range 16 to 95%). The systems were prepared by the heterophase sol–gel method. It was established that the reduction temperature increased as the silica content increased from 0 to 34% in the system, the average size of nickel crystallites being decreased from 44 to 4.5 nm. At the further increasing the silica content (to 84%): the reduction temperature decreased while the nickel crystallites grew in size to 15 nm. Testing of the prepared systems in benzene hydrogenation showed that the surface of nickel particles was accessible to the reactants.

Introduction

Nickel–silica nanosystems are widely used catalysts for various reactions of hydrogenation and hydrogenolysis. The usual method for the system preparation is wet impregnation of preformed silica gels with nickel salts, mainly nitrates.^{1–4} However, an increase in the metal loading to above 10–15% leads to formation of coarse nickel crystallites in the postreduced systems that have a detrimental effect on the system efficiency. Different mechanisms of metal particles coarsening was discussed elsewhere.^{2,5,6}

Much finer nickel particles in the amount larger than 15% in the system can be obtained using the method of deposition-precipitation of nickel hydroxide on aqueous silica suspension.^{1,7–8} If weak surface nickel–silica interaction occurs during impregnation, the deposition-precipitation leads to formation of nickel nanoparticles through the bulk phase of lamellar silicates, which are hard-to-reduce compounds.⁹ They are not completely reduced by hydrogen even at high temperatures that accounts for the small size of nickel crystallites. The standard Ni/SiO₂ catalyst comprising 50% of nickel (Euro Ni-1) prepared by deposition-precipitation is characterized elsewhere.¹⁰ The nickel crystallites are shown to remain strongly attached to the support at the reduction temperature below 500 °C (the authors referred to this state as hemispherical); they are 3.7 nm in average size, the reduction degree being 85%. When the systems are heated in hydrogen at 630–650 °C, the reduction degree reaches 96%, while the nickel particles are shaped as spheres of ca. 6 nm average size. Available literature data are mainly devoted to the nickel–silica systems comprising no more than 30 wt % of nickel.

The sol–gel method using alcoxysilanes is mainly applied to synthesize low-loaded catalysts.¹¹ Salts of corresponding metals dissolved in water-alcohol solutions are normally used as the metal precursors. A common point here is that addition of the metal salt solution to tetraethoxysilane (TEOS) is followed by hydrolysis and condensation of the latter. Therefore, the said method for preparation of metal–silica systems can be called the homogeneous sol–gel synthesis. The metal dispersion

decreases along with an increase in its content in the systems prepared by this method.¹² One can state that the homogeneous sol–gel synthesis is appropriate for preparation of noble metal containing systems but not systems containing other metals; the wetness impregnation is more appropriate for the latter. Sol–gel catalysts with low base metals content cannot compete with the impregnated catalysts because the silica produced from alcoxysilanes is more expensive than a commercial silica. Attempts of preparing dispersed high-loaded metal–silica systems (comprising the metal in amount up to 64%) have been failed since metal particles are not produced finer than 20–40 nm in average size.¹³ The heterophase sol–gel method proposed by us before^{14,15} enables to resolve this problem. The method consists of the following: Tetraethoxysilane (TEOS) is hydrolyzed in an acid medium with a small amount of water to produce short high-etherified oligomers.¹⁶ Impregnation of a porous metal precursor (oxide or hydroxide) with this solution followed by drying condenses the hydrolyzate to form polysiloxane films directly on the precursor surface and hence interphase silicate compounds can arise. The next steps of calcination and reduction lead to formation of a silica matrix with metal nanoparticles confined in its pores.

The present work demonstrates potentialities of the heterophase sol–gel method for synthesis of high-loaded metal–silica systems with particles less than 10 nm in size.

Experimental Section

A high-dispersed nickel precursor was prepared by hydrolysis of an ammonia complex produced by dissolving nickel nitrate in an aqueous ammonia solution at 20 °C. The precipitate was filtered out and washed with water in order to remove ammonium nitrate. The specific surface area of the prepared α -nickel hydroxide was 460 m²/g after drying in air at 110 °C. Nonstoichiometric nickel oxide (comprising 63% of nickel) was prepared by calcining the hydroxide in flowing air at 250 °C. The moisture capacity of the nickel oxide was 5.6 cm³/g.

Alcosol (the source of silica) was prepared by mixing 50 mL of TEOS, 40 mL of ethanol, 2 mL of water and 0.5 mL of 40% HCl. Content of silica was 0.147 g/1 mL of the solution. To

* Corresponding author. E-mail: erm@catalysis.nsk.su.

prepare NiO–SiO₂ systems, nickel oxide was impregnated with the alcosol. The required silica concentration in the system was obtained by diluting the alcosol with ethanol.^{15,17} The mixture was dried in flowing air at room temperature. Then the temperature was elevated to 150 °C, and the sample was allowed to stand at this temperature for an hour.

NiO–SiO₂ samples were reduced in the temperature-programmed mode (TPR) using a quartz U-shape reactor by heating from room temperature to 700 °C at the heating rate of 5 °C·min⁻¹, in 10% v/v H₂ in argon (the gas mixture was dehydrated by KOH). The gas mixture flow rate was set at 30 cm³/min at atmospheric pressure. The sample weighed 6 mg. The reduced samples to be characterized by physicochemical methods were passivated by ethanol.

X-ray powder diffraction patterns were recorded using a URD-63 diffractometer (CuK α radiation at $\lambda = 0.15418$ nm, a graphite crystal monochromator). Silicon was the internal reference. Coherent scattering regions were determined for nickel oxide and nickel metal by the Scherer equation based on broadening of diffraction lines (111) and (200). The microstructure of the reduced samples was studied in more detail based on full-profile analysis of the diffraction pattern comprising diffraction lines (111), (200), (220), (311), and (222).

Infrared (IR) spectra were recorded (21 scans) at room temperature using a BOMEM-MB-102 spectrophotometer. Samples were finely ground and dispersed in KBr pellets at the ratio of about 1.5 mg per 500 mg of KBr. The resolution of the IR spectra was 4 cm⁻¹.

TEM studies of the samples were carried out using JEM-2010 and JEM-100CX microscopes. A finely ground catalyst was suspended in ethanol and ultrasonically dispersed. A drop of the fine suspension was placed on a fine-mesh copper screen. A holey-carbon-coated copper grid was placed on the screen, coated side touching the droplet. Thus the droplet was allowed to evaporate leaving a uniform deposit of the catalyst on the carbon-coated side. The impregnated grid was placed in the microscope. Particle size distribution was obtained by tabulating 500 particles within specific size range. Histograms were constructed by determining the total particle percentage in each size range.

The precision adsorption measurements were carried out by static method using an ASAP-2400 (Micrometrics), for adsorption of N₂ at 77 K.

Concentration of anions in samples was determined by capillary electrophoresis using an ionic analyzer Quanta 4000E (Waters). A sample was allowed to stand in bidistilled water at boiling temperature for an hour, then the mixture was filtered and analyzed.

The reaction of benzene hydrogenation was chosen for precision measurements of the activity of nickel in the catalysts. Benzene was pre-cleaned from sulfur compounds by boiling over Raney nickel.¹⁸ Composition of the gaseous reaction mixture was as follows: 10% hydrogen, 3–4% benzene, 86–87% argon. The gas mixture flow was 20 cm³/min. The sample in the amount comprising 5–10 mg of nickel was loaded into a quartz U-shape reactor. The reaction temperature was 120 °C. The reaction rate was evaluated from variations in the heat conductivity of the outlet reaction mixture using a katharometer. The katharometer operated at 100 °C. The experimental conditions were chosen so as the hydrogen consumption was not higher than 20–25% of its content in the mixture in order to provide the stable linearity of katharometer reading. Absolute values of hydrogen consumption were obtained using calibrated argon/hydrogen mixtures. Composition of the outlet reaction

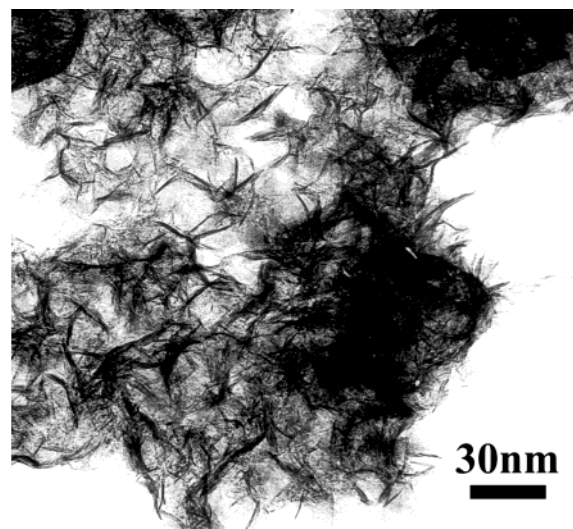


Figure 1. Micrograph of NiO (250 °C).

mixture was controlled chromatographically using helium as gas carrier and a column filled with γ -Al₂O₃.

Results and Discussion

The morphology of NiO prepared by calcining of the hydroxide at 250 °C is illustrated in Figure 1. The oxide is a pseudomorphosis of the initial substance: turbostratic nickel hydroxide. The specific surface area of the oxide was 400 m²/g. XRD data show the coherent scattering regions to be 3–4 nm in size. The formation of the poorly crystalline oxide phase at this temperature is indicated by XRD in accordance with literature data.¹⁹ Total volume of pores (from moisture capacity) was 5.6 cm³/g. The volume of pores ranging from 1 to 100 nm in size was 1.09 cm³/g (from nitrogen adsorption measurements) at the average pore size equal to 17 nm.

A series of seven samples with different silica proportions were prepared to study the nature of the interaction between the nickel oxide surface and the silica film formed upon condensation of hydrolyzed tetraethoxysilane.

It is common knowledge that the chemical interaction between a metal and the support has a crucial influence on the nucleation and final size of the metal particles formed during reduction. The nature of the interaction can be elucidated using the TPR technique. The results obtained by temperature-programmed reduction of the samples are presented in Figure 2 and in the Table 1. Two peaks of hydrogen consumption with maxima at 225 and 263 °C are observed during reduction of high-dispersed nickel oxide free of silica. It should be noticed that the first peak is only observed for NiO synthesized at temperatures below 400 °C. Mile attributes this effect to the transformation of “Ni₂O₃” into NiO.⁴ Other researchers also referred to the presence of similar nonstoichiometric oxides.²⁰ The process of Ni²⁺ transformation into Ni⁰ starts at about 240 °C and occurs within a very narrow temperature range to finish completely at 255 °C. Despite the low reduction temperature, the average size of nickel crystallites increases by an order of magnitude in comparison to the initial oxide particles (3–4 nm) to reach 44 nm.

Analysis of the TPR profile observed during reduction of sample 2 (5% SiO₂ on the basis of Ni metal) demonstrates that addition of SiO₂, even in small proportion, results in a remarkable shift toward higher reduction temperatures (350 °C), as well as in broadening of the peak of hydrogen consumption, while nickel crystallites are considerably decreased in size (from

TABLE 1: Dependence of the Reduction Temperature of Nickel–Silica Systems and the Average Size of Nickel Crystallites on the Component Ratio

samples	Ni/SiO ₂ percentage in the post-reduced system	reduction temperature, °C ^a	average size of nickel crystallites, nm TEM data	average size of nickel crystallites, nm XRD data
1	100/0	250	35	44
2	95/5	350	11	10,5
3	90/10	500	7	7,1
4	80/20	500	5,8	6,0
5	66/34	550	4,2	4,5
6	48/52	500	6,0	6,5
7	16/84	450	13,5	15

^a The reduction temperature was determined from TPR data. Reduction degree of the samples was not lower than 98%.

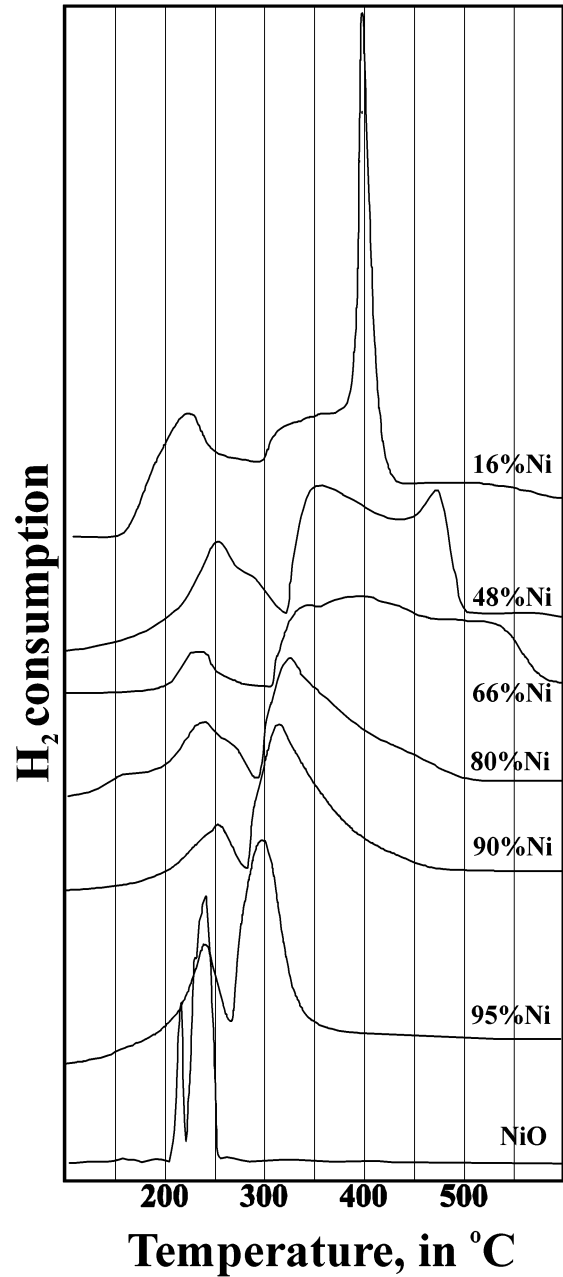


Figure 2. TPR profile obtained at reduction of nonsupported high-dispersed NiO (sample 1) and TPR profiles obtained at reduction of NiO–SiO₂ systems. Heating rate 5°/min, sample weights 6 mg, gas feeding rate 30 cm³/min.

44 to ca. 10 nm, Table 1). This trend is preserved at the further increase in the silica proportion (10, 20, and 34 wt %). According to TEM data the minimal attainable average size of

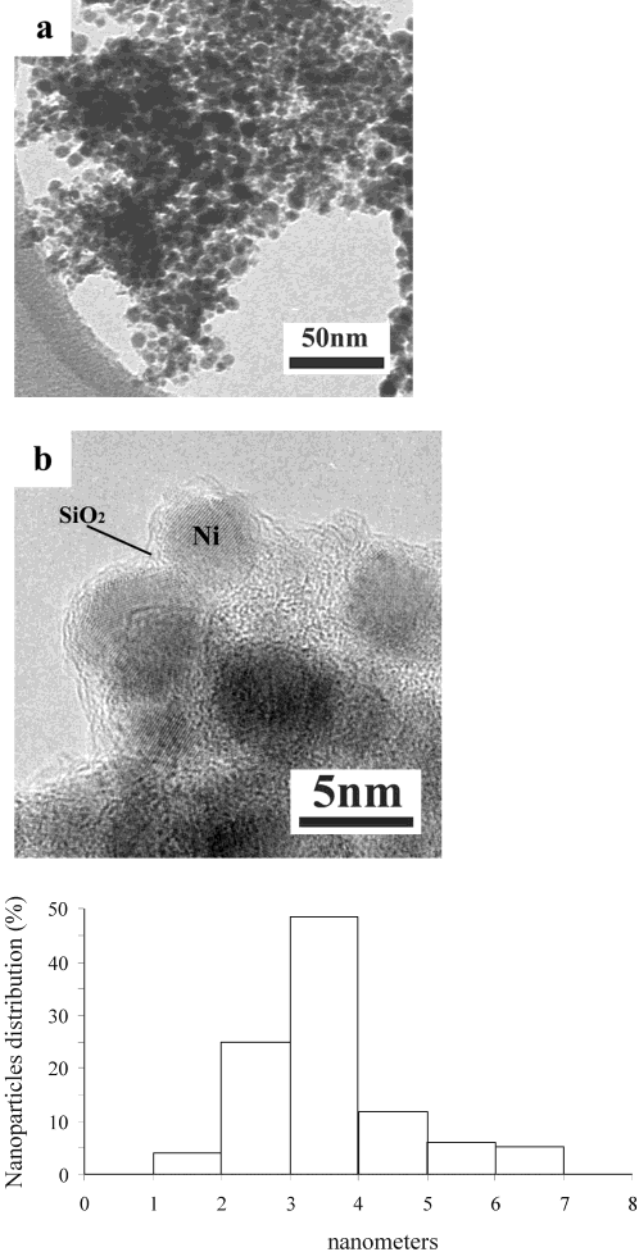


Figure 3. (a,b) Micrographs of sample 5 reduced at 550 °C and the nanoparticles size histogram.

the nickel particles equals 4.2 nm (Figure 3). The histogram of particles size distribution demonstrates that the size of 85% of nickel particles falls into the range of 2–5 nm. Thus, the stabilizing influence of silica films is seen to strengthen with an increase in the silica proportion in the system. It would be logical to suppose that the further increase in the silica content

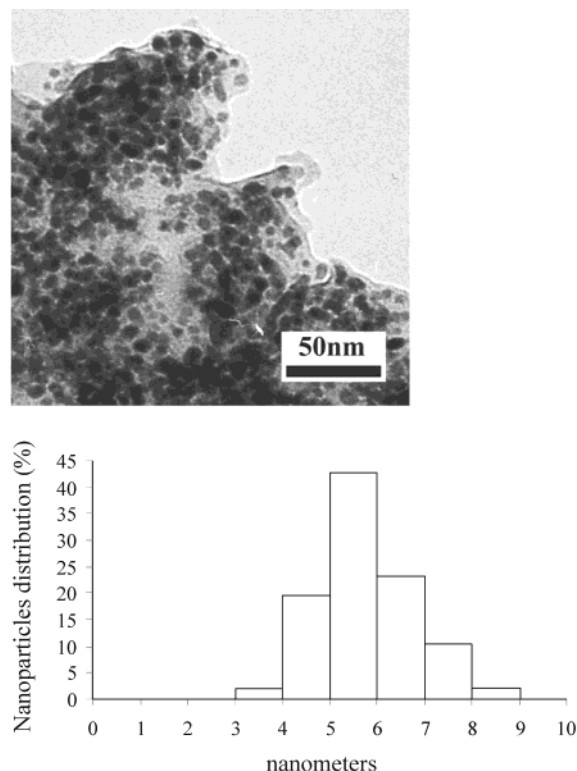


Figure 4. Micrograph of sample 6 reduced at 500 °C and the nanoparticles size histogram.

in the system results in a better isolation of the metal particles to be reduced or, at least, stops affecting the reduction process. However, TPR profiles recorded for the systems with the silica content higher than 34%, i.e., 52 and 84% (Figure 2), illustrate an anomalous trend. Two maxima become more and more apparent in the TPR curve at the range corresponding to transformation of oxide species to Ni^0 . The first of them is, as before, at the range of 300–400 °C, and the second starts appearing at 400–500 °C. In the system containing 84% of silica, the second peak is very similar to the pattern of reduction of pure nickel oxide. Notice that there occurs spontaneous reduction of remaining oxide species if the temperature elevation is stopped at 400 °C. In this case the average size of metal particles increases to 15 nm despite relatively low reduction temperature. Thus, *prima facie* a paradoxical conclusion arises that silica provides worse protection of nickel particles from sintering when introduced in amount of 84% than in amount of 5% in the system.

What is a reason for the observed phenomenon? That may be the presence of impurity anions in the system. Since HCl is used as the catalyst for TEOS hydrolysis, a part of chlorine ions may react with the nickel oxide to form nickel chloride. Capillary electrophoresis studies reveal that chlorine ions are in the amounts of 0.06, 0.1, 0.3, 0.6, 1.5, and 6 wt % in the NiO-SiO_2 systems comprising 5, 10, 20, 34, 52, and 84 wt % of silica, respectively. Hence the maximal amount of nickel chloride (1.5 and 6 wt %) is in the systems containing 52 and 84% of silica. Since nickel chloride is volatile in the presence of hydrogen, nickel particles grow during reduction due to transport of molecular species through the vapor phase.^{2,21}

XRD and TEM data show that samples 5 and 6 are the most dispersed among the samples of this series (the nickel crystallites are rather close to 4–5 and 5–6 nm in size, see Figures 3 and 4, respectively, and Table 1) while the corresponding TPR

profiles are different. In addition to nickel chloride, silicate-like phases may arise at various reduction stages when the interaction of hydrogen with nickel oxide produces water. We failed to detect silicates using XRD data on the systems treated in hydrogen at 400–450 °C. Peaks attributed to nickel or nickel oxide were only observed in the XRD patterns, their intensity ratio being dependent on the temperature of stopping the reduction. No other peak is observed. For this reason IR-spectroscopy was used for identification of the chemical bonds responsible for the dissimilar modes of the samples reduction. Figure 5 shows IR spectra recorded for the sample 5 comprising 34% of silica and for the sample 6 comprising 52% of silica (in the oxide form and reduced form). IR-spectra of SiO_2 and NiO are given for comparison. The frequency range under study for comparing IR spectra is 400–1300 cm^{-1} : this is exactly the range where changes in the absorption profile attributed to the nickel–silica interaction are observed. Absorption bands of impurity anions (1305 and 1380 cm^{-1}),²² deformation and valence vibrations of water (1630 cm^{-1} and a broad absorption band with the maximum at 3440 cm^{-1} , respectively) are observed at the range above 1300 cm^{-1} which will be not considered here since the common features are observed with all the samples. For sample 5 in oxide form it is seen that the absorption band (a.b.) at 408 cm^{-1} remains practically unchanged against that of initial NiO (250 °C) at 406 cm^{-1} but the band at 450 cm^{-1} is -5 cm^{-1} shifted relative to a.b. at 455 cm^{-1} characteristic of SiO_2 (150 °C). There are two small maxima at 560 and 615 cm^{-1} . These are absorption bands of SiO_2 (150 °C) at 583 cm^{-1} and of NiO (250 °C) at 632 cm^{-1} but shifted by -23 and -17 cm^{-1} , respectively, indicating the interaction between the system constituents. The absorption band at 795 cm^{-1} (Si-O bending vibration) is practically at the same position as the one of SiO_2 (150 °C) at 793 cm^{-1} . An unidentified low-intensity peak appears at 881 cm^{-1} . The absorption band at 950 cm^{-1} assigned to the Si-OH bond²³ is shifted to 967 cm^{-1} that argues for formation of the Ni-O-Si bond.²⁴ However, some researchers^{25,26} also attribute this band to vibration of the Si-OH bond. Notice that the main peak of silica at 1080 cm^{-1} keeps its position (cf. a.b. at 1078 cm^{-1} for SiO_2 (150 °C)). Hence, the major part of silica is not bound to nickel oxide. Seemingly the interaction between silica film and hydrated surface of nickel oxide produces surface compounds only.

No band at 429 cm^{-1} typical to NiO (450 °C) is observed in the spectrum of the sample 5, heated in hydrogen at 400 °C (incomplete reduction). Probably, all silica-unbound nickel oxide is transformed into nickel metal. A.b. at 459 cm^{-1} matches a.b. at 462 cm^{-1} of SiO_2 (600 °C). The shoulder at 653 cm^{-1} may be assigned to silicate species. Bands at 790 and 1070 cm^{-1} are shifted by -12 and -24 cm^{-1} , respectively, from bands at 802 and 1094 cm^{-1} of SiO_2 (600 °C). This is the opinion of some researchers that the shifted main band of silica indicates formation of silicate species.²⁷ They also state that this band is not shifted in the spectrum recorded for the mechanical mixture of components.

There are main absorption bands at 1070, 790 and 470 cm^{-1} in the spectrum of the samples 5 containing 34% of SiO_2 reduced at 600 °C. They are shifted by -24 , -12 and $+8 \text{ cm}^{-1}$, respectively, relative to absorption bands of SiO_2 (600 °C), viz. 1094 cm^{-1} (Si-O asymmetric stretching vibration), 802 cm^{-1} (Si-O symmetric stretching vibration) and 462 cm^{-1} (O-Si-O bending vibration). Besides, a number of low intense bands at 738, 683, and 633 cm^{-1} indicate the presence of nonreduced silicate species in small amounts.

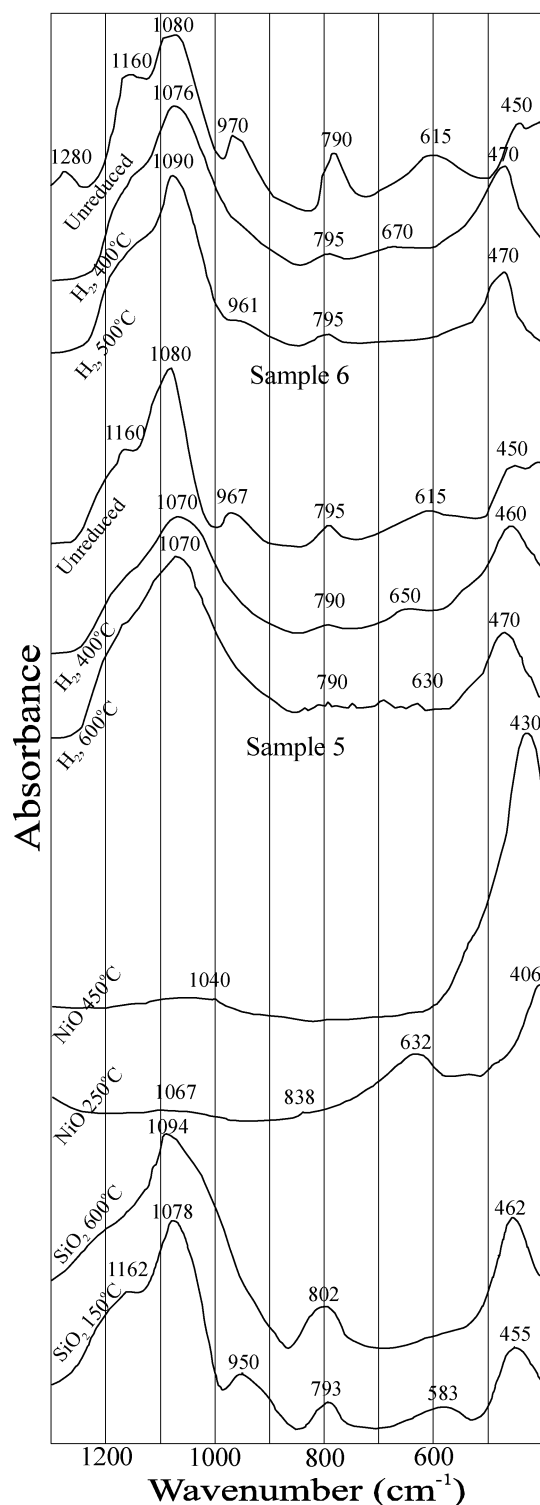


Figure 5. IR spectra of samples 5 and 6 recorded at different preparation stages. Spectra of nickel oxide (250 and 450 °C) and silica prepared by drying the hydrolizate and calcining at 150 and 600 °C are shown for comparison.

Let us examine the IR spectra of sample 6, containing 52% of SiO₂ (Figure 5). The spectrum of oxide form of sample 6 does not differ from that of oxide form of sample 5 except the lines attributed to silica are more intense. In case of reduction at 400 °C, practically identical spectra also are recorded with samples containing 34% and 52% of silica. However, if both systems are reduced completely (the former at 600 °C and the latter at 500 °C), some differences appear in the spectra at the region between 600 and 740 cm⁻¹. For the sample with higher

TABLE 2: Comparative Intensities of Diffraction Lines of the Ideal Nickel Structure and the Real Structures of Dispersed Nickel in the Reduced Samples ($\Delta(\%) = |(I_{hkl}^{ideal} - I_{hkl}^{real})100/I_{hkl}^{ideal}|$)

samples	Ni/SiO ₂ , %	intensities of diffraction lines <i>hkl</i> , B %				
		[111]	[200]	[220]	[311]	[222]
ideal fcc Ni, <i>d</i> _{Ni} = 50 Å	100	100	45.2	22.8	24.9	7.2
3	90/10 <i>d</i> _{Ni} = 75 Å	100	41	27	25	6.7
			$\Delta = 9.3\%$	$\Delta = 18.4\%$		
4	80/20 <i>d</i> _{Ni} = 60 Å	100	33	25	22	4
			$\Delta = 27\%$	$\Delta = 9.6\%$		
5	66/34 <i>d</i> _{Ni} = 45 Å	100	31	36	27	6
			$\Delta = 31.4\%$	$\Delta = 58\%$		
6	48/52 <i>d</i> _{Ni} = 65 Å	100	35	27	25	6.7
			$\Delta = 22.5\%$	$\Delta = 18.4\%$		
7	16/84 <i>d</i> _{Ni} = 150 Å	100	35	21	24	7.7
			$\Delta = 22.5\%$	$\Delta = 7.8\%$		

silica loading, no a.b. is seen in this region. The main silica bands (at 1088, 797, and 462 cm⁻¹) are less shifted from the corresponding positions of a.b. of SiO₂ (600 °C) (1094, 802, and 462 cm⁻¹), while these bands are at 1074, 792, and 471 cm⁻¹ for the sample containing 34% of silica. Hence, the sample containing 52% of silica is reduced more completely at a lower temperature than the one containing 34% of silica.

Additional data for characterization of the reduced samples are obtained by full-profile analysis of XRD patterns of the freshly reduced samples (by X-ray diffraction method, ex situ). The XRD patterns are recorded by 0.1° step scanning at the 20 s dwell time. The experimental XRD patterns are processed using a special program.²⁸ This program simulates XRD patterns on the basis of different crystal models. Along with structural parameters, real particle sizes, concentration of point, or planar defects and some others are taken into account. The appropriate models are chosen by comparing the simulated and experimental XRD patterns. This program also was used for simulation of XRD pattern for the ideal fcc structure of 5 nm nickel particles. The strength of nickel–silica interaction can be evaluated from distortion of the crystal lattice. The data obtained are summarized in Table 2. It is seen that relative intensities of diffraction lines are different for the real samples and ideal nickel, the difference being more pronounced in the case of sample 5. The difference between the unit cell constants are found; the constants are $a = 3.5238$ (for the ideal nickel lattice) and $a = 3.5280$ (for sample 5). Thus, these data argue that reduced samples contain finely dispersed nickel crystallites which are structured otherwise than the ideal fcc nickel. On the bases of the preliminary data, one can assume that in the systems under consideration the nickel metal particles include point defects which are most likely caused by incorporation of SiO₂ tetrahedrons into the metal structure. The highest proportion of these defects is observed in sample 5 that is in agreement with the TPR and IR data on the stronger interaction between the constituents of the system containing 34% of silica.

Comparison of Catalytic Activity of Ni–SiO₂ Systems to Benzene Hydrogenation. Dispersed nickel systems are often used as catalysts for hydrogenation processes. It seems interesting to test the synthesized nickel–silica systems in one of these reactions. Obviously, the high dispersion of nickel particles is of no importance if their surface is inaccessible for the reactants. The reaction of hydrogenation of benzene into cyclohexane has been studied in order to find correlation between the size of nickel particles and their exposed surface area. It is commonly known that hydrogenation of benzene is a structurally insensible reaction, and hence, the reaction rate will be proportional to the exposed nickel surface.^{3,29}

TABLE 3: Catalytic Activity of Ni–SiO₂ Systems Prepared by Sol–Gel Method to Benzene Hydrogenation at 120 °C

samples	% Ni	average size of Ni, XRD, Å	total activity, g benzene/g Ni•h	total activity, mmol benzene/g Ni•min	specific area of Ni, m ² /g	specific activity, mmol/m ² •min
1	100	440	0.767	0.164	15.3	10.7
2	95	105	3.17	0.678	64	10.6
3	90	75	3.4	0.728	90	8.1
4	80	60	4.68	0.999	112	8.9
5	66	45	5.8	1.214	150	8.1
6	48	65	4.87	1.04	103	10.1
7	16	150	1.69	0.360	45	8

^a Ni_{spec.area} = 6 × 10⁴/8.9d_A (ref 3).

Benzene hydrogenation is a highly exothermic reaction (206 kJ/mol). Calorification leads to self-heating of the catalyst bed that impedes precision activity measurement. For this reason, a low-hydrogen (10%) gas mixture has been used in order to prevent the catalyst from self-heating and, on the other hand, to provide high accuracy of the activity measurement because the hydrogen consumption for hydrogenation can be easily determined from changes in heat conductivity of the mixture. The hydrogen heat conductivity at 100°C (the katharometer temperature) is 13 times as high as that of argon, whereas heat conductivities of argon, benzene, and cyclohexane are very close to one another. Therefore, variations in the heat conductivity of the reaction mixture are only determined by a decrease in the hydrogen content. The experimental error in this case depends on the katharometer accuracy and is no more than 5%. It is well-known that almost 100% selectivity to cyclohexane is characteristic of nickel catalysts. This is also confirmed by our measurements. Only cyclohexane is detected as the hydrogenation product in the chromatogram of the outlet gas mixture.

The data in Table 3 show that the hydrogenation rate is always in good agreement with the average size of nickel particles in the catalyst, i.e., the rate increases with a decrease in the average size of nickel crystallites. The close values of specific activity observed for all the catalysts and for silica-free nickel powder indicate the accessibility of the surface of nickel particles in the systems under study.

Conclusions

Reduction of nickel–silica systems prepared by the heterophase sol–gel method over a wide concentration range (16–95 wt % Ni) was studied. TPR technique was used to establish that an increase in the silica content in the system from 0 to 34% resulted in an increase in the reduction temperature, the nickel crystallites being decreased in size from 44 to 4–5 nm (from XRD and TEM data). An unexpected effect was observed upon the further increase in the silica content, viz., the reduction temperature fell down but the nickel crystallites increased in size up to 15 nm. This effect was established to result from the presence of chlorine ions in a considerable amount (1.5–6 wt %) in the samples containing more than 34 wt % of silica.

IR spectroscopy was used to monitor genesis of two most dispersed Ni–SiO₂ systems containing 34 and 52% of silica, respectively. No remarkable difference was revealed in IR spectra recorded for the samples reduced at an intermediate temperature (400 °C). On the contrary, extra absorption bands attributed to residual silicate species were observed at 600–740 cm^{−1} in the IR spectrum of the sample containing 34% of SiO₂ (reduced at 600 °C) but not in the spectrum of the sample containing 52% of SiO₂ that indicated more complete reduction even though the reduction temperature was lower (500 °C). Besides, most pronounced distortion of the nickel lattice caused by incorporation of silicate species are characteristic of the sample comprising 34% of silica.

Thus, the whole set of data obtained using various techniques support the assumption that the highest interaction between the components is characteristic of the system containing 34% of SiO₂.

The highest dispersion of Ni–SiO₂ systems is observed at the silica concentration from 20 through 52 wt % (80 through 48 wt % of Ni, respectively). It should be emphasized that the high size uniformity of the metal particles is an important feature of these systems.

Testing of the Ni–SiO₂ systems in the reaction of benzene hydrogenation demonstrates that the catalytic activity of the systems prepared by the sol–gel method increases in proportion to a decrease in the average size of nickel particles, i.e., the nickel surface is accessible to the reactants.

The current state of art allows heterophase sol–gel synthesis to be considered a new and very promising method for preparation of high-loaded nickel–silica catalysts.

Acknowledgment. The authors are grateful to Dr. G. N. Kustova for the IR data, Dr. A. L. Chuvilin for the TEM data, and Dr. A. F. Danilyuk for helpful discussion.

References and Notes

- (1) Dzisko, V. A.; Karnaukhov A. P.; Tarasova D. V. *Physicochemical Principles of Synthesis of Oxide Catalysts*; Nauka: Novosibirsk, 1978; p 348.
- (2) Wynblatt, P.; Gjostein, N. A. *Prog. Solid State Chem.* **1974**, 9, 21.
- (3) Borekov, G. K. *Heterogeneous Catalysis*; Nauka: Moskva, 1986; p 258.
- (4) Mile, B.; Stirling, D.; Zammit, M. A.; Lovell, A.; Webb, M. J. *Catal.* **1988**, 114, 217.
- (5) Roman, A.; Delmon, B. *J. Catal.* **1973**, 30, 333.
- (6) Ruckenstein, E.; Pulvermacher, B. *J. Catal.* **1973**, 29, 224.
- (7) Hemans, L. M.; Geus, J. W. In *Preparation of Catalysts II*; Delmon B., Grange P., Jacobs P. A., Poncelet G., Eds.; Elsevier: Amsterdam, 1979; p 113.
- (8) Coenen, J. W. E. *Appl. Catal.* **1989**, 54, 65.
- (9) Burattin, P.; Che, M.; Louis, C. *J. Phys. Chem.* **2000**, 104, 10482.
- (10) Coenen, J. W. E. *Appl. Catal.* **1991**, 75, 193.
- (11) Gonzalez, R. D.; Lopez, T.; Gomez, R. *Catal. Today* **1997**, 293.
- (12) Ennans, G.; Mei, A.; Musinu, A.; Pinna, G.; Solinas, S. *J. Non-Cryst. Solids* **1998**, 232–234, 587.
- (13) Ernst, B.; Libs, S.; Chaumette, P.; Kiennemann, A. *Appl. Catal.* **1999**, 186, 145.
- (14) Ermakova, M. A.; Ermakov, D. Yu.; Kuvshinov, G. G.; Plyasova, L. M. *Kinet. Katal.* **1998**, 5, 791.
- (15) Ermakov, D. Yu.; Ermakova, M. A.; Kuvshinov, G. G. Russia Patent 2126718, Borekov Institute of Catalysis, 1999.
- (16) Brinker, C. J.; Assink, R. A. *J. Non-Cryst. Solids* **1989**, 111, 48.
- (17) Ermakova, M. A.; Ermakov, D. Yu.; Kuvshinov, G. G.; Plyasova, L. M. *J. Catal.* **1999**, 187, 77.
- (18) Graul, R. J.; Karabinos, J. V. *Science* **1946**, 104, 557.
- (19) Bihan, S. Le.; Figlarz, M. *Thermochim. Acta* **1973**, 6, 319.
- (20) Garner, W. E. *Chemistry of the Solid State*; University of Bristol: London, 1955.
- (21) Hoang-Van, C.; Kachaya, Y.; Teichner, S. G.; Arnaud, Y.; Dalmon, J. A. *Appl. Catal.* **1989**, 46, 281.
- (22) Burratin, P.; Che, M.; Louis, C. *J. Phys. Chem. B* **1997**, 101, 1060.
- (23) Ro, J. C.; Chung, J. J. *J. Non-Cryst. Solids* **1991**, 130, 8.

- (24) Ueno, A.; Suzuki, H.; Kotera, Y. *J. Chem. Soc., Faraday Trans. 1* **1983**, 79, 127.
- (25) Kermarec, M.; Carrial, J. Y.; Burattin, P.; Che, M. *J. Phys. Chem. B* **1994**, 98, 12008.
- (26) Lopez, T.; Romero, A.; Gomez, R. *J. Non-Cryst. Solids* **1991**, 127, 105.
- (27) Sviderskiy, V. A.; Voronkov, M. G.; Klimenko, V. S.; Klimenko, S. V. *Zhurnal prikladnoi khimii* **1997**, 70, 1698.
- (28) Cherepanova, S. V.; Tsybulya, S. V. *J. Mol. Catal. A* **2000**, 158, 263.
- (29) Satterfield, C. N. In *Heterogeneous Catalysts in Practice*; McGraw-Hill: New York, 1980.